HAL
open science

A coupled numerical/experimental investigation of a turbulent rotor-stator flow

Eric Séverac, Sébastien Poncet, Eric Serre, Marie-Pierre Chauve

To cite this version:

Eric Séverac, Sébastien Poncet, Eric Serre, Marie-Pierre Chauve. A coupled numerical/experimental investigation of a turbulent rotor-stator flow. 8th ISAIF, Jul 2007, Lyon, France. pp.ISAIF8-006. hal-00170266

HAL Id: hal-00170266

https://hal.science/hal-00170266v1

Submitted on 7 Sep 2007

HAL is a multi-disciplinary open access archive for the deposit and dissemination of scientific research documents, whether they are published or not. The documents may come from teaching and research institutions in France or abroad, or from public or private research centers.

L'archive ouverte pluridisciplinaire **HAL**, est destinée au dépôt et à la diffusion de documents scientifiques de niveau recherche, publiés ou non, émanant des établissements d'enseignement et de recherche français ou étrangers, des laboratoires publics ou privés.

Proceedings of the 8th International Symposium
on Experimental and Computational
Aerothermodynamics of Internal Flows
Lyon, July 2007
Paper reference: ISAIF8-006

A coupled numerical/experimental investigation of a turbulent rotor-stator flow

Eric Séverac, Sébastien Poncet, Eric Serre, Marie-Pierre Chauve*

MSNM-GP, UMR 6181, Technopôle Château-Gombert, 38 rue F. Joliot-Curie, 13451 Marseille – France
*IRPHE, UMR 6594, Technopôle Château-Gombert, 49 rue F. Joliot-Curie, BP 146, 13384 Marseille – France

Turbulent incompressible flows are studied both numerically and experimentally within an annular rotor-stator cavity of aspect ratio G=(b-a)/h=5 and radius ratio a/b=0.286 (where a and b are the inner and outer radii of the rotating disk and h the interdisk spacing). Besides its fundamental importance as a three-dimensional prototype flow, such flows are crude models of flows arising in many industrial devices, especially in turbomachinary applications. Our aim is to investigate turbulent regimes at three Reynolds numbers $Re=\Omega b^2 / \nu=10^5$, 4×10^5 and 10^6 (Ω the rotation speed of the rotor and ν the kinematic viscosity of the fluid) corresponding to different flow properties as the rotation of the rotor is increased. Experimental measurements have been obtained using a laser Doppler anemometer (LDA) technique. Numerical modelling is based on a Large Eddy Simulation (LES) using a spectral vanishing viscosity (SVV) technique implemented in a Chebyshev-collocation Fourier-Galerkin pseudo-spectral code. As far as the authors are aware, LES of fully turbulent flow in an actual shrouded rotor-stator cavity have not been performed before. Turbulent quantities are shown to compare very favourably with experimental measurements and are shown of interest in understanding the physics of turbulent rotor-stator flows from transitional to turbulent regimes. Moreover, averaged results may provide target data for workers employing RANS schemes.

Keywords: Rotor-stator flows, Turbulent rotating flows, Large Eddy Simulation

Introduction

Rotating disk flows have been the subject of a constant interest because of their relevance for the turbine engineering field [11]. Besides its primary concern to industrial applications, the rotor-stator problem has also proved a fruitful means of studying turbulence in confined rotating flows. Indeed, rotating disk flows are among the simplest flows where the boundary layers are three-dimensional from their inception and they are therefore well suited for studying the effects of mean-flow three-dimensionality on the turbulence and its structure.

According to the combination of the rotation speed Ω and the interdisk spacing *h*, the present study concerns a flow with two boundary layers flow separated by a core (Batchelor flow) [12, 14]. Experiments of Itoh *et al.* [5] have revealed that transition to turbulence first appears within the Bödewadt layer on the stator, even though the flow remains laminar in the Ekman layer along the rotor. Itoh *et al.* [5] reported a turbulent regime occurring along the stator side at $Re_r= \Omega r^2 / \nu =8\times10^3$ (r the local radius), while along the rotor side, turbulent flow develops later for $3.6\times10^5<Re_r< 6.4\times10^5$ for G=12.5. Differences in

Eric SEVERAC: PhD student

turbulence characteristics between the rotor and stator sides have also been observed and attributed to the effects of the radial convective transport of turbulence.

Thus, the structure of these flows is highly complex involving laminar, transitional and turbulent flow regions. Moreover, as a consequence of confinement, flow curvature and rotation effects, the turbulence is strongly inhomogeneous and anisotropic. Consequently, these flows are very challenging for turbulence modelling which is today the only numerical approach able to investigate turbulent flows in industrial conditions. Indeed, the turbulence model must be able to solve the region of low Reynolds number not only near the discs but also in the core of the flow. Moreover, the model has to predict precisely the location of the transition from the laminar to the turbulent regime, even though the transition process is bounded by instabilities, and so cannot be completely represented by a steady flow model. One of the most important failures of eddy viscosity models in predicting this type of flow is an overestimate of the extent of the relaminarized zone on the inner part of the rotating disc [3,4], leading to erroneous Ekman layer predictions and the rotation rates in the central core. Second moment closures provide a more appropriate level of modelling to predict such complex flows [7, 14], but even if they provide a correct distribution of laminar and turbulent regions, the Reynolds stress behaviour is not fully satisfactory, particularly near the rotating disc. The improvement of these turbulence models is a great challenge.

Consequently, the LES seems the appropriate level of modelling. To our knowledge, there exists only two interesting studies using LES [1, 11, 19]. Wu & Squires [21] performed LES of the three-dimensional turbulent boundary-layer over a free rotating disk at Re = 6.5×10^5 and in an otherwise quiescent incompressible fluid using periodic boundary conditions both in the radial and tangential directions. In an angular section of a cavity homogeneous in the radial direction, Lygren & Andersson [1, 11] performed LES for Reynolds numbers ranging from Re = 4×10^5 to Re = 1.6×10^6. All these LES results supported the view of Littell & Eaton [8] that the mean flow three-dimensionality affects the near wall vortices and their ability to generate shear-stresses.

Turbulent regimes are investigated here in a closed annular rotor-stator cavity, using experimental measurements as well as Large-Eddy Simulation based on Spectral Vanishing Viscosity (SVV).

Geometry

The cavity is composed by two parallel disks of radius b=140mm, one rotating at a uniform angular velocity Ω (rotor), one being at rest (stator). The disks are delimited by an inner cylinder (the hub) of radius a=40 mm attached to the rotor and by an outer stationary casing (the shroud) slightly larger than the rotor. The cavity is filled with water maintained at a constant working temperature 20°C.

In the following, the stator is located at z*=z/h=1 and the rotor at z*=0. We define also the dimensionless radial location as r*=(r-a)/(b-a).

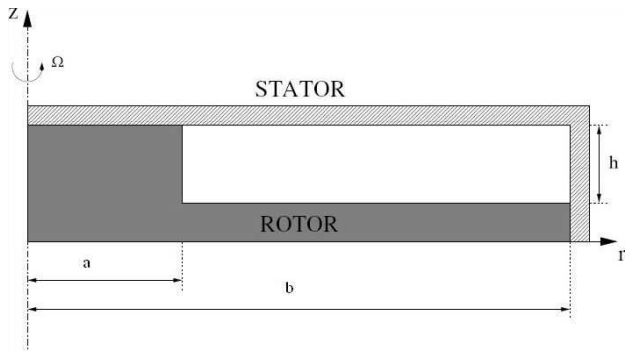

Fig. 1 Experimental apparatus and relevant notation.

Instrumentation and measurements

The measurements are performed using a two component laser Doppler anemometer (LDA). The LDA technique is used to measure from above the stator the mean radial V_r and tangential V_θ velocities as well as the associated three Reynolds stress tensor components in a vertical plane (r,z): $R^*_{rr} = \overline{v_r'^2}/(\Omega r)^2$, $R^*_{\theta\theta} = \overline{v_\theta'^2}/(\Omega r)^2$ and $R^*_{r\theta} = \overline{v_r' v_\theta'}/(\Omega r)^2$. This method is based on the accurate measurement of the Doppler shift of laser light scattered by small particles (Optimage PIV Seeding Powder, 30 μm) carried along with the fluid. Its main qualities are its non intrusive nature and its robustness. About 5000 validated data are necessary to obtain the statistical convergence of the measurements. It can be noticed that, for small values of the interdisk space h, the size of the probe volume (0.81mm in the axial direction) is not small compared to the boundary layer thicknesses and to the parameter h.

Numerical modelling

The incompressible fluid motion is governed by the three-dimensional Navier-Stokes equations written in primitive variables (see below).

$$\begin{aligned} &\frac{\partial \mathbf{V}}{\partial t} + (\mathbf{V}\cdot\nabla)\mathbf{V} = \nabla p + \frac{1}{Re}\Delta\mathbf{V} && \text{in } D \\ &\nabla\cdot\mathbf{V} = 0 && \text{in } \overline{D} = D\cup\Gamma \\ &\mathbf{V}\big|_{\Gamma=\partial D} = W \end{aligned} \tag{1}$$

where t is the time, **V** is the velocity of components (u,v,w) in the radial, tangential, and vertical direction respectively, for cylindrical coordinates (r, θ, z), p is the pressure. This equation is completed by initial conditions for the velocity:

$$\begin{aligned} &\mathbf{V} = \mathbf{V}_0 \\ &\nabla\cdot\mathbf{V}_0 = 0 \text{ in } \overline{D} \end{aligned} \tag{2}$$

The scales for the dimensionless variables of space, time and velocity are h/2, Ω^{-1}, Ωb, respectively. No-slip boundary conditions are applied at all walls. The tangential velocity is fixed to 0 on the stator and on the external cylinder and to the local disk velocity on the rotor and the hub. The singularity at the junction of the outer cylinder at rest with the rotor (or the rotating inner cylinder with the stator) is regularized by using an exponential function to provide a smooth switchover.

The temporal discretization is a projection scheme, based on backwards differencing in time (see all the details in Raspo *et al.* [16]). The specificity of the algorithm is to allow a temporal evolution of the normal pressure gradient at the boundaries. The temporal scheme is second-order semi-implicit combining an implicit second order backward Euler scheme for the diffusive terms and an explicit Adams-Bashforth extrapolation for the non-linear convective terms.

A collocation Chebychev approximation is used in both radial and axial non-homogeneous directions associated with Gauss-Lobatto points. A standard Fourier-Galerkin approximation is employed in the 2π-periodic direction. We note that $N_2/2$ is the cut off frequency of the Fourier series. For each Fourier mode, the solution is approximated by Chebychev polynomials of degree N_1 and N_3, in the radial and axial direction, repsectively. Finally, a full diagonalization technique is used for solving a set of 2D uncoupled Helmholtz and Poisson problems obtained after splitting the Euler scheme to group the implicit part in the left hand side of the equations.

The LES is performed through a Spectral Vanishing Viscosity technique (SVV) [6, 13, 20]. In the frame of collocation method, an appropriate viscosity operator is incorporated in the Helmholtz equations of velocity prediction, only active for high wave numbers of the numerical approximation. This operator does not affect the large scales of the flow and stabilise the solution by increasing the dissipation, particularly near the cut off frequency. According to the literature [6, 20], we choose to define our SVV operator as follow:

$$\begin{aligned} &\tilde{\Delta} V_N \equiv \nabla.\left((\nabla V_N)\times Q_N\right) \\ &\text{with } Q_N \equiv diag\left\{Q^i_{N_i}\right\} \end{aligned} \tag{3}$$

where the 1D operator is only defined in spectral space as a C^∞ smooth function:

$$\begin{aligned} &\hat{Q}^i_{N_i}(\omega) \equiv \varepsilon^i_{N_i}.\chi_{]\omega^i_T,\omega^i_C]}.e^{-\left(\frac{\omega^i_c-\omega}{\omega^i_T-\omega}\right)^2} \\ &\varepsilon^i_{N_i} = O\left(\frac{1}{N_i}\right) \\ &\omega^i_T = O\left(\sqrt{\omega^i_c}\right) \end{aligned} \tag{4}$$

where Q_N denotes the 3D SVV operator that is composed of three 1D SVV operators $Q^i_{N_i}$; *i*=1, 2, 3 corresponding to the r, θ, z, directions respectively; the operator is parameterized by $\varepsilon^i_{N_i}$ the maximum of viscosity and ω^i_T the threshold after which, the viscosity is applied. ω^i_C is the highest frequency calculated in the direction i. Because our SVV operator is fully linear, it is gathered with the implicit standard diffusion term. Consequently, no additional computational cost is needed.

Table 1 Computational parameters

Re	ω_T	ε_N	Grid	δt
10^5	3N/4 (r-direction)	1/(2N)	81	10^{-4}
	N/2 (θ-direction)	1/(2N)	150	
	√N (z-direction)	1/(2N)	49	
4 x 10^5	0.8√N	1/(2N)	121	10^{-4}
	√N	1/(2N)	181	
	√N	1/(2N)	65	
10^6	2√N	1/N	151	10^{-5}
	5√N	1/N	241	
	4√N	1/N	81	

The computational parameters used in the present LES are summed up in table 1. Let's notice that in order to increase the azimuthal resolution, some calculations at Re=10^6 have bee carried out in a half-cavity, thus forcing a π-periodicity of the solution.

Results

Note that all the quantities have been normalized by the local velocity of the rotor Ω*r*. The statistical data have been averaged in time and in the homogeneous tangential direction.

To identify the critical value of the rotational Rey-

nolds number for the transition to turbulence along the stator, we have performed some flow visualizations using a CCD video camera situated one meter above the stator. The cavity has been seeded with reflective particles of kalliroscope (30 x 6 x 0.07 μm). Figure 2 presents two visualizations at $Re=4.1\times10^4$ and $Re=10^5$. For the lowest value of the Reynolds number, the spiral patterns denoted SR1 by Schouveiler *et al.* [17] have almost disappeared. For increasing values of Re up to 10^5, the turbulent structures get always thinner and the Bödewadt layer along the stator is clearly turbulent for $Re=10^5$. This is consistent with the previous results of Randriamampianina and Poncet [14], who obtained by DNS and for the same Reynolds number a turbulent regime along the stator, whereas the Ekman layer along the rotor remains laminar. In the following, we focus only on the turbulent regime $Re\geq10^5$.

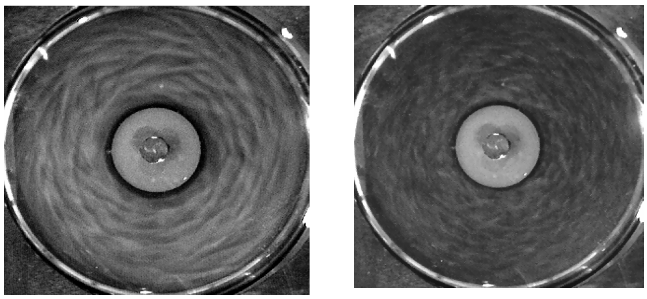

Fig. 2 Flow visualizations from above the stator for (a) $Re=4.1\times10^4$ and (b) $Re=10^5$.

- *Base flow*. As for an infinite disc, when the upper disc is impulsively started, a thin Ekman boundary layer is formed which acts as a pump drawing in fluid axially and driving it away in centrifugal spirals (this is sometimes known as 'Ekman pumping'). In a closed container, this fluid swirls along the stationary vertical outer wall to the stationary disc. Then, the fluid spirals inward in the Bödewadt layer before again turning axially towards the rotating disc. Consequently, at moderate rotation rates, the base flow is steady and axisymmetric and of Batchelor type with both Ekman and Bödewadt layers separated by a non-viscous core rotating at constant angular velocity [12].

- *Turbulent flows*. The turbulent flows have been investigated at three Reynolds numbers $Re=10^5$, $Re=4\times10^5$, and $Re=10^6$ corresponding to different flow properties. For the three Reynolds numbers considered in this study, the *mean flow* (Fig. 3) is broadly a Batchelor flow as in the laminar regime, with two boundary layers separated by a core in solid body rotation. Indeed, on average, there exists a main flow in the tangential direction coupled with a secondary flow in the (r, z) plane.

As expected, the thicknesses of both boundary layers (at mid-radius) decrease when increasing Ω (Figure 3). The Ekman boundary layer thickness can indeed be scaled by $\delta=(\nu/\Omega)^{1/2}$, the thickness of the boundary layer over a single rotating disk. By conservation of mass, the Bödewadt boundary layer thickness behaves like the Ekman one. Note that the Bödewadt layer is almost twice thicker than the Ekman layer. On the other hand, the mean velocity in the core, denoted $K=V_\theta(z^*=0.5)/(\Omega r)$ and known as the entrainment coefficient of the fluid, slightly increases with the rotation speed. The LES computations predict K equal to 0.348 for $Re=10^5$ and 0.368 for $Re=4\times10^5$. All these values are consistent with the values found in the literature [12, 14]. The agreement between the numerical results and the measurements is very satisfactory for the mean field. The LES catches the main features of turbulent rotor-stator flows such as the thinning of the boundary layers for increasing values of Re. At $Re=10^6$, the agreement is still globally satisfying with an underestimation of only 6.33% of K.

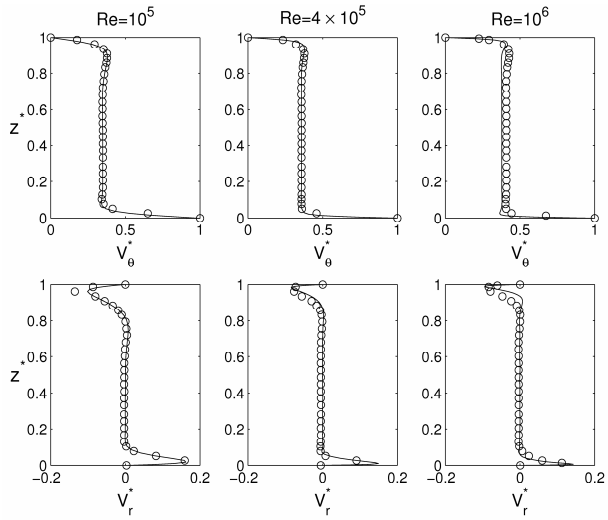

Fig. 3 Axial profiles of the mean radial and tangential velocity components. Comparisons between numerical (solid lines) and experimental (circles) statistical data at mid-radius.

A polar plot of the tangential and radial mean velocity components is shown in Figure 4 at two radial positions. As expected, it appears that the turbulence level on the rotor side is smaller than the one on the stator side. The polar plot falls indeed very close to the laminar similarity Von Kármán solution along the rotor, whereas the profile along the stator is close to the DNS results of Lygren and Andersson [9] obtained for an open turbulent rotor-stator flow. When one approaches the periphery of the cavity ($r^*=0.9$), the turbulence intensities increase as the local Reynolds number is increased and the polar profile gets closer to the turbulent profile of [10]. The LES result exhibits a less characteristic triangular form than the DNS of Lygren & Andersson [10] indicating a

weaker three-dimensionality of the flow. This difference can be explained by the large difference in Reynolds numbers and also by the confinement.

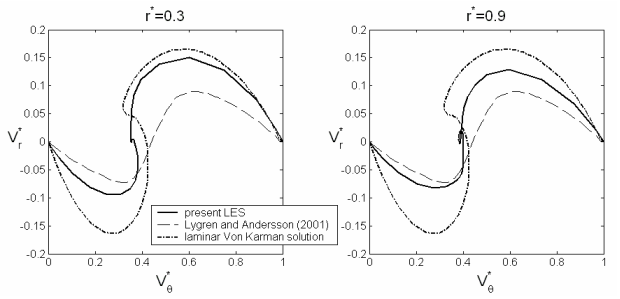

Fig. 4 Polar plot of the velocity distribution in the whole gap between the two disks at Re=10^6. Comparison between (---) the LES results, (-.-) the laminar Von Kármán solution, and (- -) the DNS results of Lygren and Andersson [10].

The main Reynolds-stress components have been accurately computed and axial profiles are shown at mid-radius in Figure 5. An examination of the off-diagonal Reynolds stresses from LES results shows that these normal stresses are dominant. Over the range of considered Reynolds numbers, the numerical profiles fit quite well the experimental measurements both in the boundary layers and in the core. The experimental values are nevertheless generally lower than the simulated ones. This is particularly true at Re=4×10^5 as already observed in DNS at the same Reynolds number by Lygren & Andersson [10] with the experimental measurements of Itoh *et al.* [5]. The presence of the shroud in the experiment cannot be invoked here.

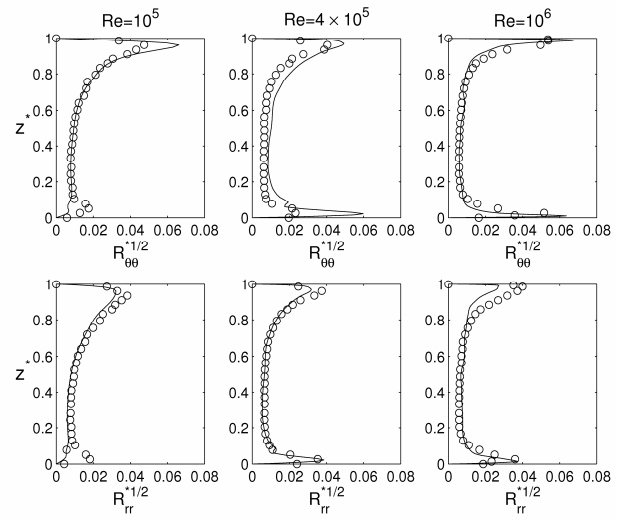

Fig. 5 Axial profiles of two normal components of the Reynolds stress tensor. Comparisons between numerical (solid lines) and experimental (circles) statistical data at mid-radius.

At Re=10^5, the flow regime is transitional turbulent, characterized by a fully turbulent stationary disk layer and a laminar rotating disk layer (Fig.5), which confirms the flow visualizations shown in fig.2 and the numerical and experimental data of Randriamampianina and Poncet [14]. This can be seen also from the iso-surface of the Q-criterium in both boundary layers (fig.6a,b). On the rotor, the turbulence is confined along the rotating hub and in the Stewartson layer along the external cylinder.

By increasing further the Reynolds number up to Re=4×10^5 and Re=10^6, both boundary layers are turbulent at mid-radius (fig.5), whereas the core remains laminar. This was expected from the experiments of Itoh *et al* [5], where the rotating layer became turbulent for $Re_r = 3.6\times10^5$. At Re=4×10^5 the turbulence intensity is larger on the rotor than on the stator in the LES results, as already mentioned by Lygren & Andersson [10] in DNS. This could be here a consequence of a more efficient turbulence transport in our LES than in our experiment, where the gap between the rotating inner cylinder and the stator would be able to decrease the turbulence intensity of the rotor inflow. Note also that the turbulence intensities decreased along the stator for increasing values of Re from 10^5 to 4×10^5. The increase in the rotation rate leads indeed to a broader range of turbulent scales and to a progressive reduction in turbulence intensities with a smaller level of anisotropy between components. The same features have long been known in plane channel flow, too. At Re=4×10^5, the rotating disk layer is only turbulent at large radii, corresponding to the largest values of local Reynolds number. At smaller radii, a view of the coherent structures in the flow (Fig.6c) shows large spiral arms characteristics of the unstable laminar flow and related to crossflow instability. These spirals were already observed in transitional regimes both numerically and experimentally. As soon as the turbulence occurs, these structures are broken, giving rise to smaller and more axisymmetric structures. These structures are similar to the ones observed on the fully turbulent stator (Fig.6d) and on the both layers at Re=10^6 (Fig.6e,f).

Figure 7 present the axial variations of the six Reynolds stress tensor components at mid-radius and for Re=10^6. It confirms the anisotropy in the normal stresses deduced from Figure 5. The normal stress is greatest in the tangential direction, exceeding by a factor of about 3 the one in the radial direction in the Bödewadt layer. Let's notice that this anisotropy in the normal stresses is stronger in LES. This difference between the components decreases when increasing Reynolds number (Fig.5). The three components, which include the axial velocity fluctuations, are negligible (Fig.7). Note that the experimental values of the $R_{r\theta}^*$ component are very close to zero (not represented here), whereas the LES predicts a strong shear stress in both boundary layers.

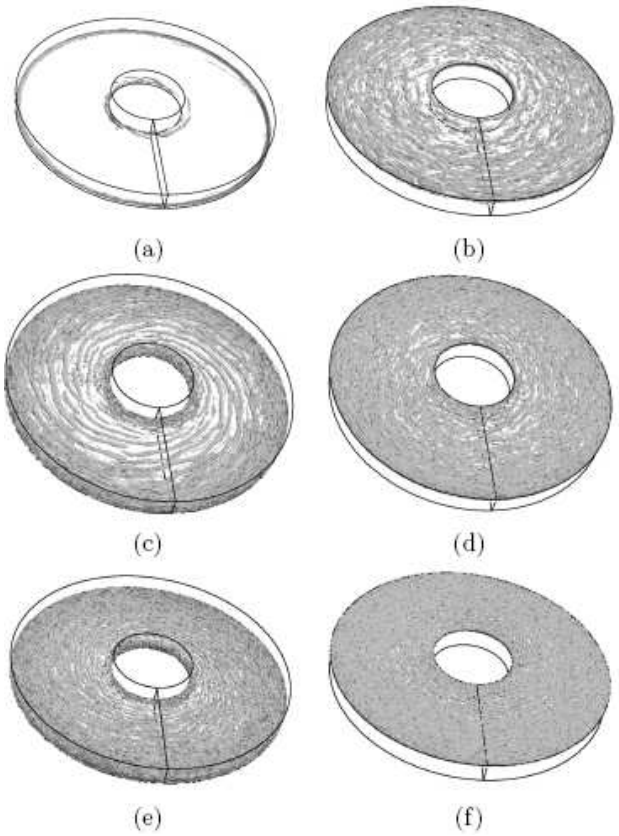

Fig. 6 Iso-surface of the Q-criterium along the rotor (a,c,e) and along the stator (b,d,f) for (a,b) Re=10^5, (c,d) Re=4×10^5, (e,f) Re=10^6.

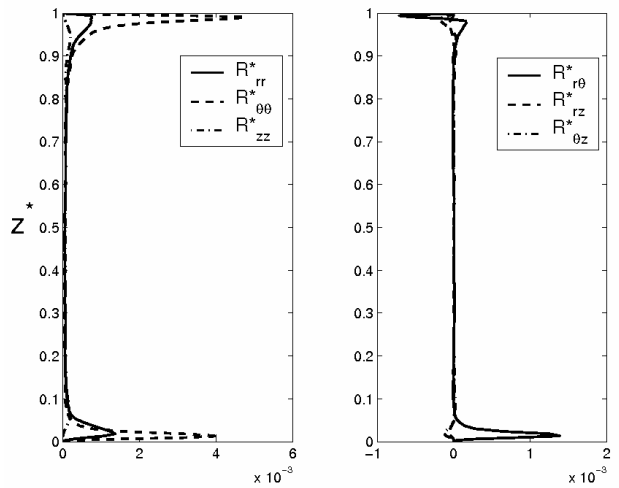

Fig. 7 Axial variations of the Reynolds stress tensor componentts for Re=10^6 and r*=0.5.

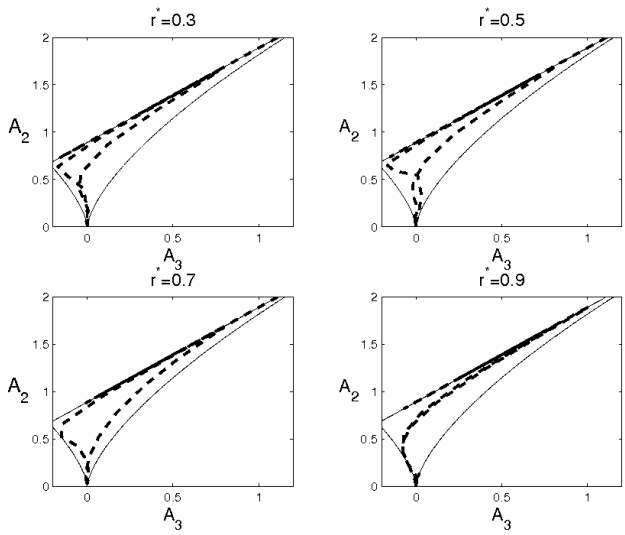

Fig. 8 Anisotropy invariant map for Re=10^6 at four radial locations. Dashed lines: LES, solid lines, realizability diagram of Lumley [9].

Figure 8 presents the anisotropy invariant map for Re=10^6. The second A_2 and third A_3 invariants of the anisotropy tensor a_{ij} of the second moments of the fluctuations are defined as: $A_2= a_{ij}\, a_{ji}$ and $A_3= a_{ik}\, a_{kj}\, a_{ji}$, where $a_{ij} =R_{ij}/k-2/3\delta_{ij}$ (k the turbulence kinetic energy and δ_{ij} the Kronecker symbol). The results of the LES respect the realizability diagram of Lumley [9] as they remain within the region delimited by the three solid lines. Close to the disks, the turbulence tends to follow the two-component behavior ($A_3= A_2-8/9$) as the wall normal fluctuations are damped more effectively than fluctuations parallel with the disks. At the edge of the Ekman layer, for $0.3 \leq r^* \leq 0.7$, the third invariant gets negative and close to the limit (-2/9, 2/3). Then, the turbulence tends to the axisymmetric limit ($A_3=- A_2^{3/2}/\sqrt{6}$). Moreover, as $R_{\theta\theta}$* is much larger than the other normal components of the Reynolds stress tensor (Fig.7), one may indentify cigar-shaped vortex very elongated in the axial direction. One interesting feature is that closer to the shroud (r*=0.9) where high turbulence level prevails, these vortex disappear, which is due to the confinement. Whatever the radial location, the turbulence is fairly close to the isotropic case ($A_2= A_3=0$) in the core of the flow.

One characteristics of the three-dimensional turbulent boundary layer is the reduction of the Townsend structural parameter $a_1=\tau / (2k)$, defined as the ratio of the shear stress vector magnitude τ to twice the turbulent kinetic energy k [10]. We have reported in figure 9 the variation at four radial locations of a_1 in wall units z^+ in both boundary layers. We can see clearly a significant reduction below the limiting value 0.15 for a two-dimensional turbulent boundary layer, with behaviors similar to those reported by Itoh *et al.* [5] and Littell

and Eaton [8] from their measurements. It suggests the three-dimensional turbulent nature of the flow along the rotor and stator walls [8]. This reduction of a_1 indicates also that the shear stress in this type of flow is less efficient in extracting turbulence energy from the mean field. Note that $a_1 > 0.15$ is obtained only very locally on the inner and outer cylinders.

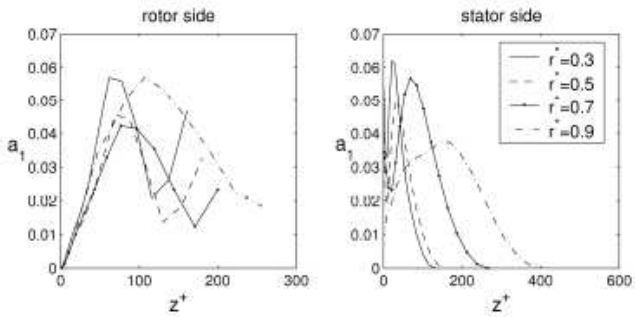

Fig. 9 Townsend structural parameter on both disks for Re=10^6.

To fix the three-dimensional nature of the boundary layers, we display in figure 10 the axial variations of the three characteristic angles in wall coordinates z^+: the mean velocity angle γ_m=arctan(V_r/V_θ), the mean gradient velocity angle γ_g =arctan($\frac{\partial V_r/\partial z}{\partial V_\theta/\partial z}$) and the turbulent shear stress angle γ_τ=arctan($\overline{v'_r\, v'_z}/\overline{v'_\theta\, v'_z}$). The profile of γ_m clearly shows the continuous change of direction of the mean velocity vector with the distance from the wall, one of the major characteristics of three-dimensional turbulent boundary layer. The angle remains in the range $-1° < \gamma_m < 17°$ within the Ekman layer and in the range $-34° < \gamma_m < 1°$ within the Bödewadt layer. Another feature of 3DTBL is that the direction of the Reynolds shear stress vector in planes parallel with the wall is not aligned with the mean velocity gradient vector. Such a misalignment is observed in the present LES on both disks. The lag between γ_τ and γ_g is large towards the boundary layers with a maximum value about 100° on the rotor to be compared with the value 18° reported by Lygren and Andersson [10] in infinite disk system. In their numerical study of non-stationary 3DTBL, Coleman *et al.* [2] obtained large values of the lag especially near the wall and inferred it from the slow growth of the spanwise component of the shear stress. These authors observed also the change of the sign of the gradient angle γ_g. Such large values of this lag make the assumption of eddy-viscosity isotropy to fail for the prediction of such flows. In the present case, this feature indicates a strong three-dimensionality with highly distorted flow field resulting from the shear induced by rotation over the disks, adding another complexity in comparison with the idealized configuration in Lygren and Andersson [9].

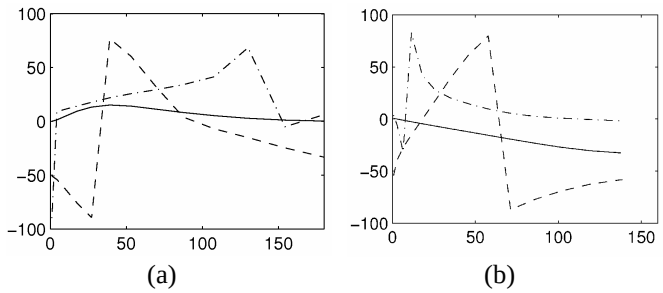

Fig. 10 Axial evolutions of the three characteristic angles in wall units for Re=10^6 at r*=0.5: (a) along the rotor side, (b) along the stator side. (solid lines) γ_m, (dashed lines) γ_g, (dashed-dotted lines) γ_τ.

Concluding remarks

In this paper, Large Eddy Simulation and experimental measurements of turbulent rotor-stator flows are presented for three Reynolds numbers in the range [10^5;10^6] in order to show the complexity of the flow when rotation has been increased.

At this stage, the experimental measurements have validated the numerical modelling of the rotor-stator problem at large rotation rates. Consequently, these numerical results occur to be the first from LES of an enclosed rotor-stator flow. All the results show that turbulence is inhomogeneous and anisotropic. It highlights the weak potential of closure models based on isotropic eddy viscosity to produce reliable results in such configuration. The three-dimensional nature of both layers has also been demonstrated.

Acknowledgement

The authors acknowledge the IDRIS (CNRS) computing centre (program 060242). The authors are very grateful to Professors R. Pasquetti (CNRS/ Lab. J. Dieudonné Nice) and B.E. Launder (Univ. of Manchester) for fruitful discussions. The work was supported by CNRS in the frame of the DFG-CNRS program “LES of complex flows”. Support for E. Séverac by a CNRS grant is also acknowledged.

References

[1] Andersson H.I., Lygren M., LES of open rotor-stator flow, Int. J. Heat Fluid Flow, vol.27, pp.551-557, (2006).

[2] Coleman G.N., Kim J., Spalart P.R., A numerical study of strained three-dimensional wall-bounded turbulence, J. Fluid Mech., vol.416, pp.75-116, (2000).

[3] Crespo del Arco E., Serre E, Bontoux P. & Launder B., Stability, transition and turbulence in rotating cavities,. Edited by: M. RAHMAN, Dalhousie University Canada Series: Advances in Fluid Mechanics 41, 2005.

[4] Iacovides H., Theofanoupolos I.P., Turbulence modelling of axisymmetric flow inside rotating cavities, Int. J. Heat Fluid Flow, vol.12, pp.2-11, (1991).

[5] Itoh M., Yamada Y., Imao S., Gonda M., Experiments on turbulent flow due to an enclosed rotating disc, Expl Thermal Fluid Sci., vol.5, pp.359-368, (1992).

[6] Karamanos G. S., Karniadakis G. E., A spectral vanishing viscosity method for large eddy simulation, J. Comp. Phys., vol.163, pp.22-50, (2000).

[7] Launder B. E., Tselepidakis, D. P., Application of a new second moment closure to turbulent channel flow rotating in orthogonal mode, Int. J. Heat Fluid Flow, vol.15, pp.2-10, (1994).

[8] Littell H.S., Eaton, J.K., Turbulence characteristics of the boundary layer on a rotating disk, J. Fluid Mech., vol.266, pp.175-207, (1994).

[9] Lumley J.L., Computational modelling of turbulent flows, Adv. Appl. Mech., vol.18, pp.123-176, (1978).

[10] Lygren M., Andersson H., Turbulent flow between a rotating and a stationary disk, J. Fluid Mech., vol.426, pp.297-326, (2001).

[11] Lygren M., Andersson H., Large eddy simulation of the turbulent flow between a rotating and a stationary disk, ZAMM, vol.55, pp.268-281, (2004).

[12] Owen J. M., Rogers R., H., Flow and heat transfer in rotating-disc systems, Vol. 1: Rotor-stator sytems, Research Studies Press, Taunton, (1989).

[13] Pasquetti R., Xu C. J., High-order algorithms for large-eddy simulation of incompressible flows, J. of Sci. Comp., vol.17, pp.273-284, (2002).

[14] Poncet S., Chauve M.-P., Schiestel R., Batchelor versus Stewartson flow structures in a rotor-stator cavity with throughflow, Phys. Fluids, vol.17, 075110, (2005).

[15] Randriamampianina A., Poncet S., Turbulence characteristic of the Bödewadt layer in a large enclosed rotor-stator system, Phys. Fluids, vol.18, 055104, (2006).

[16] Raspo I., Hugues S., Serre E., Randriamampianina A., Bontoux P., Spectral projection methods for the simulation of complex three-dimensional rotating flows, Computers and Fluids, vol.31, pp.745-767, (2002).

[17] Schouveiler L., Le Gal P., Chauve M.P., Instabilities of the flow between a rotating and a stationary disk, J. Fluid Mech., vol.443, pp.329-350, (2001).

[18] Serre E., Bontoux P., Launder B., Direct numerical simulation of transitional turbulent flow in a closed rotor-stator cavity, Flow, Turbulence & Combustion, vol.60, pp.35-50, (2002).

[19] Séverac E., E. Serre, P. Bontoux & B.E. Launder. “A Spectral Vanishing Viscosity Technique as Large Eddy Simulation of Transitional Rotor-Stator Flows”, 6th European Conference on Turbo-machinery, proceedings vol2 (Ed.: G. Bois, C. Sieverding, M. Manna, T. Arts), p740-749 (ref: 072_06/187), Lille(France) 2005.

[20] Séverac E., Serre E., Bontoux P., Launder B.E., Large eddy simulation of transitional rotor-stator flows using a spectral vanishing viscosity technique, ERCOFTAC Series 10: 217-224. Lamballais, E. (Eds): Direct and Large-Eddy Simulation VI. Spinger-Verlag, (2006).

[21] Wu X., Squires K.D., Prediction and investigation of the turbulent flow over a rotating disk, J. Fluid. Mech., vol.418, pp.231-264, (2000).